Influence of Coulomb Interactions on the Properties of Induced Pairing Model

W.R. Czart and St. Robaszkiewicz

Institute of Physics, Adam Mickiewicz University
Umultowska 85, 61-614 Poznań, Poland

(Received May 18, 2001)

We study the superconducting properties of a model of coexisting itinerant carriers and local pairs with finite binding energy, taking into account the effects of Coulomb (density–density) and direct pair hopping interactions. The evolution of the phase diagrams and superfluid characteristics with electron concentration, interaction parameters and the relative position of the bands is examined. The model is found to exhibit several kinds of superconducting behaviors ranging from the BCS-like to the local-pair-like. The relevance of the obtained results to the interpretation of experimental data for the doped bismuthates ($Ba_{1-x}K_xBiO_3$ and $BaPb_{1-x}BiO_3$) is pointed out.

PACS numbers: 74.20.–z, 74.20.Mn, 71.28.+d, 74.25.Ha

1. Introduction

In Ref. [1] we have reported preliminary results concerning electromagnetic and thermodynamic properties of the model introduced in Ref. [2] and called the induced pairing model, which describes the system of coexisting itinerant carriers (c-subsystem) and local pairs with finite binding energy (d-subsystem) and which is a generalization of the (hard-core) boson–fermion model [3–9].

Here we present further results on this subject and examine the effects of Coulomb (density–density) interactions and the direct pair hopping interaction which were not considered in the previous work. We will determine the phase diagrams and superconducting characteristics of the system considered as a function of total electron concentration ($n = n_c + n_d$), interactions and the relative position of the bands (Δ_0) within the approach which treats the on site interaction of localized electrons U_d exactly, and the remaining interactions within the broken symmetry Hartree–Fock approximation (HFA).

2. General formulation

The effective Hamiltonian of coexisting localized d-electrons and itinerant c-electrons analyzed in the present work, taking into account the orbital coupling of electrons to the external magnetic field, can be written as

$$H = H_d + H_c + H_{cd}, \tag{1}$$

where

$$H_d = \sum_i (E_d - \mu) n_i^d + U_d \sum_i n_{i\uparrow}^d n_{i\downarrow}^d - \frac{1}{2} \sum_{ij} \left(J_{ij} \exp(\mathrm{i}2\Phi_{ij}) \rho_i^+ \rho_j^- + \mathrm{h.c.} \right), \tag{2}$$

$$H_c = t \sum_{ij\sigma} \left(\exp(\mathrm{i}\Phi_{ij}) c_{i\sigma}^+ c_{j\sigma} + \mathrm{h.c.} \right) - \sum_i \mu\, n_i^c + \frac{1}{2} \sum_{ij} V_{ij}^c n_i^c n_j^c, \tag{3}$$

$$H_{cd} = \frac{I_0}{2N} \sum_{ikk'} \left(\exp[\mathrm{i}(k-k')R_i] c_{k\uparrow}^+ c_{-k'\downarrow}^+ \rho_i^- + \mathrm{h.c.} \right) + \frac{1}{2} \sum_{ij} V_{ij}^{cd} n_i^c n_j^d, \tag{4}$$

$n_i^c = \sum_\sigma c_{i\sigma}^+ c_{i\sigma}$, $n_i^d = \sum_\sigma d_{i\sigma}^+ d_{i\sigma}$, $\rho_i^+ = (\rho_i^-)^+ = d_{i\uparrow}^+ d_{i\downarrow}^+$, E_d measures the relative position of d-level with respect to the bottom of the c-electron band ϵ_k^c in the absence of interactions, μ is the chemical potential which ensures that a total number of particles is constant, i.e.

$$n = n_c + n_d = \left(\sum_i \langle n_i^c \rangle + \sum_i \langle n_i^d \rangle \right) / N, \tag{5}$$

U_d is the effective on-site density interaction between d-electrons, J_{ij} is the intersite charge exchange interaction of d-electrons (pair hopping), t is the hopping integral for c-electrons and I_0 is the intersubsystem charge exchange coupling. $V_{ij}^c = U_c^0 \delta_{ij} + V_{ij}^c (i \neq j)$ and V_{ij}^{cd} are the Coulomb interactions between c-electrons and those between c- and d-electrons, respectively. The Peierls factors in (2) and (3) account for the coupling of electrons to the magnetic field via its vector potential $\boldsymbol{A}(\boldsymbol{r})$, $\Phi_{ij} = (-e/\hbar c) \int_{R_i}^{R_j} \mathrm{d}\boldsymbol{r} \boldsymbol{A}(\boldsymbol{r})$, and e is the electron charge.

In analysis we have used, as in our previous works [1, 2], the variational approach which treats the on-site interaction term U_d exactly [10] and the intersubsystem and intersite interactions within the broken symmetry HFA [4]. For $\boldsymbol{A} = 0$ the resulting expression for the free energy of the superconducting phase (S) is

$$\frac{F_0^S}{N} = -\frac{2}{\beta N} \sum_k \ln \left(2 \cosh \frac{\beta A_k}{2} \right) - \frac{1}{\beta} \ln 2 Z_d + \mu(n_d + n_c) - 2\mu + C, \tag{6}$$

where

$$C = J_0(\rho_0)^2 + 2|I_0| x_0 \rho_0 - U_c^0 (x_0)^2 + (U_c/2 + U_{cd}) n_c - \frac{1}{4} U_c n_c^2$$
$$- U_{cd} n_c n_d + U_{cd} n_d + \Delta_0, \tag{7}$$

$$A_k = \left(\lambda_k^2 + |U_c^0 x_0 - I_0 \rho_0|^2 \right)^{1/2}, \quad \Delta = \sqrt{\bar{\mu}^2 + (J_0 \rho_0 + |I_0| x_0)^2}, \tag{8}$$

$$Z_d = \exp(\beta U_d/2) + \cosh\beta\Delta, \quad \lambda_k = \epsilon_k^c - \widetilde{\mu},$$

$$\Delta_0 = E_d + U_d/2, \quad J_0 = \sum_{j\neq i} J_{ij}, \quad \beta = (k_{\mathrm{B}}T)^{-1},$$

$$\overline{\mu} = \mu - \Delta_0 - U_{cd}n_c, \quad \widetilde{\mu} = \mu - \frac{1}{2}U_c n_c - U_{cd}n. \tag{9}$$

$$\rho_0 = \frac{1}{N}\sum\langle\rho_i^+\rangle \quad \text{and} \quad x_0 = \frac{1}{N}\sum_k\langle c_{k\uparrow}^+ c_{-k\downarrow}^+\rangle \tag{10}$$

are the order parameters for d- and c-subsystems, respectively. $\epsilon_k^c = -t\gamma_k$, $\gamma_k = 2\sum_\alpha \cos k_\alpha$, $\alpha = x, y, \ldots$, $U_c^0 = V_{ii}^c$, $U_c = 2V_{q=0}^c$, $U_{cd} = V_{q=0}^{cd}$, where $V_q^{c(cd)} = \sum_j V_{ij}^{c(cd)} \exp[\mathrm{i}\boldsymbol{q}\cdot(\boldsymbol{R}_i - \boldsymbol{R}_j)]$.

Upon minimizing this free energy with respect to the variables ρ_0, $2x_0$, and μ we obtain the following self-consistent equations:

$$x_0 = (U_c^0 x_0 - |I_0|\rho_0)\frac{1}{2N}\sum_k \frac{1}{A_k}\tanh\frac{\beta A_k}{2}, \tag{11}$$

$$\rho_0 = (J_0\rho_0 + |I_0|x_0)\,\frac{\sinh\beta\Delta}{2\Delta p Z_d}, \tag{12}$$

$$n = n_c + n_d, \tag{13}$$

where n_c and n_d are given by

$$n_c - 1 = -\frac{1}{N}\sum_k \frac{\epsilon_k^c - \widetilde{\mu}}{A_k}\tanh\frac{\beta A_k}{2}, \tag{14}$$

$$n_d - 1 = \frac{\bar{\mu}\sinh\beta\Delta}{\Delta Z_d}. \tag{15}$$

The energy gaps in the c-electron spectrum and the d-electron spectrum are given by $E_g^c(T) = \min(2A_k)$ and $E_g^d(T) = \Delta$, respectively, whereas $E_g^{\min}(T) = \min\{E_g^c(T), E_g^d(T)\}$ defines the minimum energy gap. The free energy of the normal (N) state F_0^N is obtained from (6) by putting $x_0 = \rho_0^x = 0$, and with μ given by $\partial F_0^N/\partial\mu = 0$.

For a weak static potential the expectation value of the Fourier transform of the total current operator can be obtained from the linear response theory as

$$J_\alpha(\boldsymbol{q},\omega) = N\frac{c}{4\pi}\sum_{\alpha'}\left[\delta_{\alpha\alpha'}K^{\mathrm{dia}} + K_{\alpha\alpha'}^{\mathrm{para}}(\boldsymbol{q},\omega)\right]A_{\alpha'}(\boldsymbol{q},\omega) \tag{16}$$

and the diamagnetic part of kernel has the following form:

$$K_\alpha^{\mathrm{dia}} = K_c + K_d, \tag{17}$$

where

$$K_c = \frac{8\pi e^2}{\hbar^2 c^2 a}\frac{1}{N}|t|\sum_{\boldsymbol{k}\sigma}\langle c^+_{\boldsymbol{k}\sigma}c_{\boldsymbol{k}\sigma}\rangle\cos(k_\alpha)$$

$$= \frac{8\pi e^2}{\hbar^2 c^2 a N}|t|\sum_{\boldsymbol{k}}\left[1-\frac{\lambda_{\boldsymbol{k}}}{A_{\boldsymbol{k}}}\tanh(\beta A_{\boldsymbol{k}}/2)\right]\cos k_\alpha, \tag{18}$$

$$K_d = \frac{32\pi e^2}{\hbar^2 c^2 a}\frac{1}{zN}\langle -\sum_k J_k\rho^+_k\rho^-_k\rangle = \frac{32\pi e^2}{\hbar^2 c^2 a}\left(-\frac{J_0(\rho_0)^2}{z}\right), \tag{19}$$

z is the number of nearest neighbors ($z=2$ for $d=1$ chain, $z=4$ for $d=2$ square lattice, $z=6$ for simple cubic lattice), a is the lattice constant. $\rho^{\pm}_{\boldsymbol{k}}$, and $J_{\boldsymbol{k}}$ are the space-Fourier transform of $\rho^{\pm}_i$ and J_{ij}, respectively, and ρ_0, x_0, and μ are determined by Eqs. (11–13).

In the static limit and $q \to 0$ for the transverse part of the paramagnetic kernel we obtain

$$K^{\rm para}_{xx}(\omega=0) = \frac{8\pi e^2 t^2}{\hbar^2 c^2 a}\frac{1}{N}\sum_{\boldsymbol{k}}\frac{\sin^2 k_x}{k_{\rm B}T\cosh^2(\beta E_k/2)}. \tag{20}$$

In the London superconductors the magnetic field penetration depth λ is determined by the transverse part of the total kernel in the static limit

$$\lambda = \left\{-K^{\rm dia} - K^{\rm para}_{xx}(\omega=0)\right\}^{-1/2}. \tag{21}$$

Using the value of the penetration depth and the difference of the free energy between N and S phase one is able to determine the thermodynamic critical field $H_{\rm C}$, the Ginzburg–Landau (G–L)correlation length ξ and the Ginzburg ratio κ as $H^2_{\rm C}(T)(8\pi) = (F^N(T) - F^S(T))/(Na^3)$, $\xi = \Phi_0/(2\pi\sqrt{2}\lambda H_{\rm C})$, $\kappa = \lambda/\xi$, where $\Phi_0 = hc/2e$, and to obtain the estimations for the critical fields $H_{c1} \simeq (\ln\kappa/\kappa)\,H_{\rm C}$ and $H_{c2} \simeq \Phi_0/2\pi\xi^2$.

From Eqs. (11–13) one can calculate the HFA transition temperature T_c at which $x_0 \to 0$ and $\rho_0 \to 0$. The $T_{\rm c}$ is given by a set of equations

$$\begin{cases} \frac{1}{2}\left(J_0 - I_0^2\frac{S}{1-U^0_c S}\right)B = 1, \\ \qquad n-2 = \bar{\mu}B - G, \end{cases} \tag{22}$$

where

$$B = \frac{\sinh\beta_c\bar{\mu}}{\bar{\mu}\left[\exp\left(\frac{\beta_c}{2}U_d\right)+\cosh\beta_c\bar{\mu}\right]}, \qquad G = \frac{1}{N}\sum\tanh\frac{\beta_c}{2}(\epsilon^c_k - \widetilde{\mu}),$$

$$S = \frac{1}{2N}\sum\frac{\tanh\frac{\beta_c}{2}(\epsilon^c_k-\widetilde{\mu})}{\epsilon^c_k-\widetilde{\mu}}.$$

3. Results of numerical solution and discussion

We have performed an extended numerical analysis of Eqs. (6–22) both at $T = 0$ and for $T > 0$, taking a rectangular density of states for c-electrons ($N(\epsilon) = 1/2D$ for $0 < \epsilon_k^c < 2D$, and 0 otherwise, with $2D$ denoting an effective c-bandwidth). In the following we summarize the main results, concentrating on the phase diagrams and basic superconducting characteristics, derived for several most representative cases.

3.1. Ground state diagrams

In the model considered there are two types of mechanisms which can lead to superconductivity. The first one is due to the direct local pair hopping interaction J and involves exclusively the narrow band subsystem. For $U_d < 0$ it gives rise to a superconductivity analogous to superfluidity of ^{4}He.

The second one is due to the intersubsystem charge exchange I_0. This leads to a superconducting state involving both subsystems, in which the single-particle spectrum of the wide band electrons opens up a gap around the position of the narrow band of electrons in pair states [2–8].

Figures 1 and 2 show the evolution of the ground state phase diagrams as a function of n and Δ_0/D obtained for $-\infty \leq U_d \leq 0$ and several fixed values of J_0, I_0, U_c, and U_{cd}.

Depending on the relative concentration of "c" and "d" electrons, which is determined by $\Delta_0 = E_0 + U_d/2$, the interactions and n, we distinguish three essentially different physical situations. In the most interesting case of $I_0 \neq 0$ (Fig. 2) it will be: (i) d-regime, $n_d \gg n_c$ (LP), (ii) $d + c$ regime, $2 > n_c$, $n_d > 0$ (MIXED), (iii) c-regime, $n_c \gg n_d$ (BCS). In d-regime the superconducting properties of the system are analogous (at least for $U_d \leq 0$) to those of pure local-pair superconductor, whereas in c-regime the situation is similar to the BCS case: pairs of "c" electrons with opposite momenta and spins are exchanged via virtual transitions into empty d-levels. In $d + c$ regime the system shows features which are intermediate between those of pure local-pair superconductor and those of classical BCS systems, even in the strong attraction ($U_d \ll 0$) case. This concerns, among others, the gap in the single-particle excitation spectrum for c-electrons, the ratio $k_B T_c/E_g(0)$, the electromagnetic coherence length as well as the thermodynamic critical field (see Sec. 3.2).

As for the evolution of the superconducting properties with an increasing total number of carriers, there are three possible types of change-over: (i) BCS$\longrightarrow$ "Crossover" (MIXED)$\longrightarrow$BCS, (ii) BCS$\longrightarrow$LP, and (iii) LP$\longrightarrow$BCS (comp. Fig. 2). Only in the case when the local pair level is deeply located below the bottom of the wide c band ($\Delta_0 \ll 0$), the system remains in d-regime for any $n \leq 2$.

Let us also observe that with the increase in Δ_0/D at fixed n there are two sequences of change-overs possible: LP$\rightarrow$ MIXED$\rightarrow$ BCS (if $n < 2$) and BCS$\rightarrow$ MIXED$\rightarrow$LP (if $n > 2$).

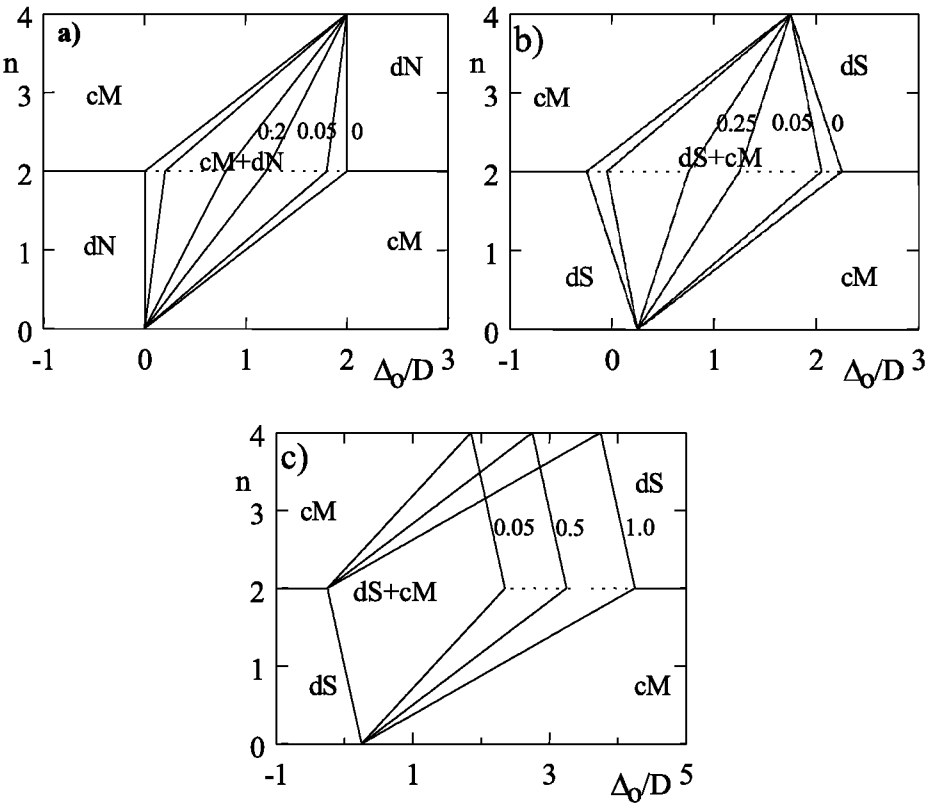

Fig. 1. Ground state diagrams of the model (1) as a function of n and Δ_0/D plotted for $-\infty \leq U_d \leq 0$, $I_0 = 0$ and different values of $J_0/2D$, $U_c/2D$, $U_{cd}/2D$, showing the effects of increasing Coulomb interactions U_c and U_{cd}; (a) $J_0/2D = 0$, $U_c/2D = 0$, $U_{cd}/2D = 0$; 0.05; 0.2 (numbers to the curves-n.t.c.); (b) $J_0/2D = 0.25$, $U_c/2D = 0$, $U_{cd}/2D = 0$; 0.05; 0.25 (n.t.c.); (c) $J_0/2D = 0.25$, $U_c/2D = 0.05$; 0.5; 1 (n.t.c.), $U_{cd}/2D = 0$. Notation: cM (metallic state of c-electrons), dN (normal state of d-electrons), dS (superconducting state of d-electrons).

In contrast to the change-overs MIXED$\longleftrightarrow$ BCS, which are quite sharp, the evolution between the LP and MIXED regimes for $I_0 \neq 0$ is rather smooth (comp. Figs. 4, 5) and therefore the LP/MIXED boundary cannot be precisely located on the n vs. Δ_0/D diagrams.

In the case $I_0 = 0$, $J_0 \neq 0$, for which the ground state diagrams are shown in Fig. 1, the situation is simpler. The superconducting state is restricted to the regions marked by dS and $dS + cM$, and all the phase boundaries on the diagram are well defined. At the border $dS + cM/dS$: $n_c \to 0$ (for $n < 2$), or $n_c \to 2$ (for $n > 2$), whereas at the border $dS + cM/cM$: $n_d \to 0$ (for $n < 2$), or $n_d \to 2$ (for $n > 2$).

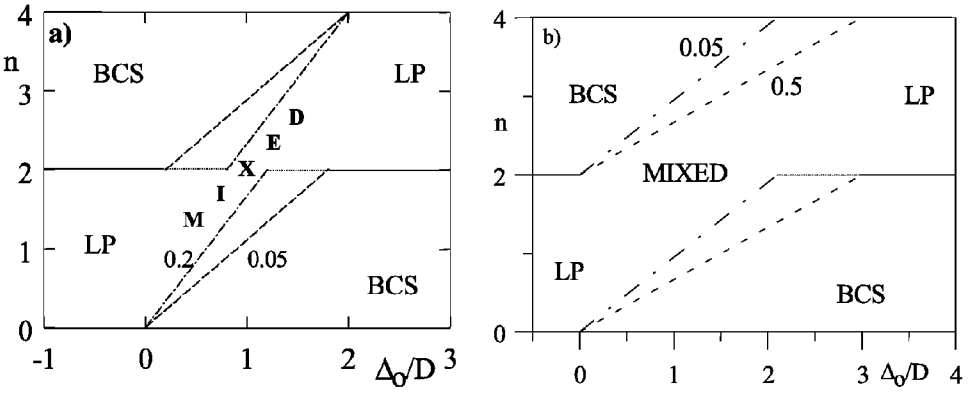

Fig. 2. Ground state diagrams as a function of n and Δ_0/D plotted for $-\infty \leq U_d \leq 0$, $J_0 = 0$, $I_0/2D = 0.1$ and different values of $U_{cd}/2D$, $U_c/2D$; (a) $U_{cd}/2D = 0.05$, 0.2 (numbers to the curves-n.t.c.), $U_c/2D = 0$, (b) $U_c/2D = 0.05$, 0.5 (n.t.c.), $U_{cd}/2D = 0$. BCS, LP, and MIXED denote superconducting state of predominantly c-electrons, d-electrons and coexisting $c + d$ electrons, respectively. By dashed lines we mark the values of Δ_0/D and n for which n_d or $2 - n_d$ become vanishingly small ($n_d/n = 10^{-5}$) defining in this way the approximate border MIXED/BCS.

As it follows from the diagrams shown in Figs. 1c, 2b the intrasubsystem Coulomb interaction U_c enlarges the coexistence region of local pairs and wide band electrons ($n_d \neq 0$, $n_c \neq 0$) expanding it towards higher values of Δ_0/D, both, in the case of $I_0 = 0$, $J_0 \neq 0$ (cf. Fig. 1c) as well as in the case of $J_0 = 0$, $I_0 \neq 0$ (cf. Fig. 2b), and the concentrations of both types of particles change smoothly with varying Δ_0.

The influence of the intersubsystem Coulomb repulsion U_{cd} is more drastic as it tends to reduce the coexistence region (cf. Figs. 1a, b, for $I_0 = 0$, and Fig. 2a, for $I_0 \neq 0$). For $U_{cd}/2D < 0.5$, D being the half-bandwidth of c-electron band, changes in the concentrations of both types of carriers, n_c and n_d versus Δ_0 are smooth. On the other hand for $U_{cd}/2D > 0.5$ discontinuous changes in n_c and n_d with variation of Δ_0 and (or) temperature can take place, and the $d+c$ (MIXED) regime can be completely suppressed. It remains an open question whether such behavior in the case of strong intersubsystem Coulomb repulsion is an inherent property of the model or if it is due to the approximation used.

3.2. Superconducting properties

Let us first conclude the evolution of basic superfluid characteristics with the particle concentration n and Δ_0/D at $T = 0$, $U_d \leq 0$. Examples of the plots of H_c^2, ξ, $1/\lambda^2$ and κ vs. n and vs. Δ_0/D are shown in Figs. 3 and 4, respectively, for the fixed values of I_0 and J_0 ($U_c = U_{cd} = 0$).

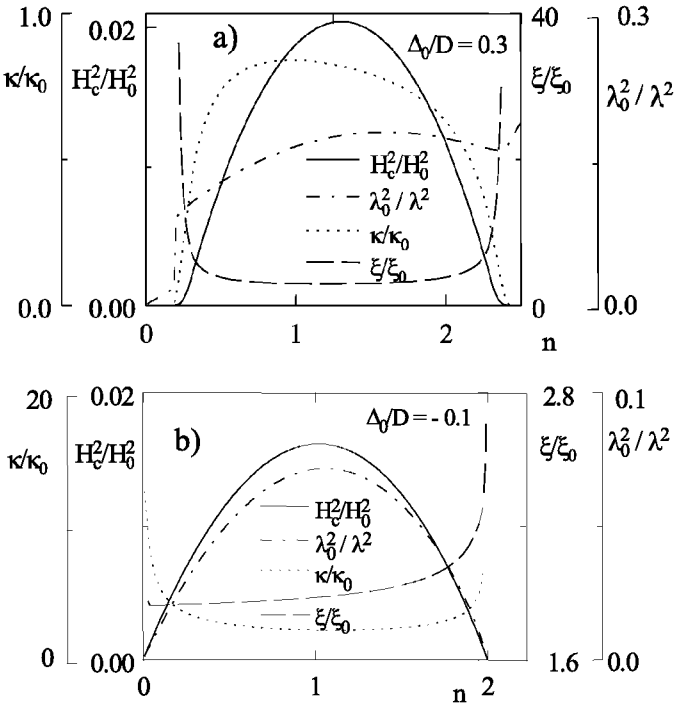

Fig. 3. Concentration dependences of H_c^2, ξ, $1/\lambda^2$, and κ at $T = 0$ for $I_0/2D = 0.1$, $J_0/2D = 0.05$, $-\infty \leq U_d \leq 0$, $U_c = U_{cd} = 0$, (a) $\Delta_0/D = +0.3$, (b) $\Delta_0/D = -0.1$. $H_0^2 = 16\pi D/a^3$, $\xi_0 = a/4\sqrt{2}$, $\lambda_0^2 = \hbar^2 c^2 az/16\pi e^2 D$, $\kappa_0 = \left(\sqrt{2}\hbar c/\sqrt{\pi}e\right)\left(1/\sqrt{aD}\right)$, $D = zt$.

In Fig. 3 we show the evolution of the thermodynamical critical field H_c, the coherence length ξ and the Ginzburg ratio $\kappa = \lambda/\xi$ and $1/\lambda^2$ with electron concentration $n = n_d + n_c$, for two fixed values of Δ_0/D and $0 \leq U_d$.

For $\Delta_0/D = 0.3$ and $I_0 \neq 0$ (Fig. 3a) upon increasing n the system exhibits two change-overs: from the c-regime (BCS) ($n_c \gg n_d \approx 0$) into the $c+d$ (MIXED) regime and then again into the c-regime (BCS) ($n_c \approx n-2$, $n_d \approx 2$). Notice only a weak n-dependence of λ, ξ, and κ in a wide range of n. This is due to a strong pinning of μ around the d-level (Δ_0) in the $c+d$ regime, which yields n_c to be almost n-independent.

For $\Delta_0/D = -0.1$ (Fig. 3b) $n_d \gg n_c$ (except $n \approx 2$ and $n > 2$) and electromagnetic characteristics for $n < 2$ are dominated by the d-subsystem. With increasing n the system exhibits a single change-over from the predominantly d-regime (LP) directly into the c-regime (BCS) at $n \approx 2$. One can observe it in the behavior of ξ, which substantially increases near $n = 2$. In comparison to the former case ξ is strongly reduced, whereas λ and κ — strongly enhanced (κ up to

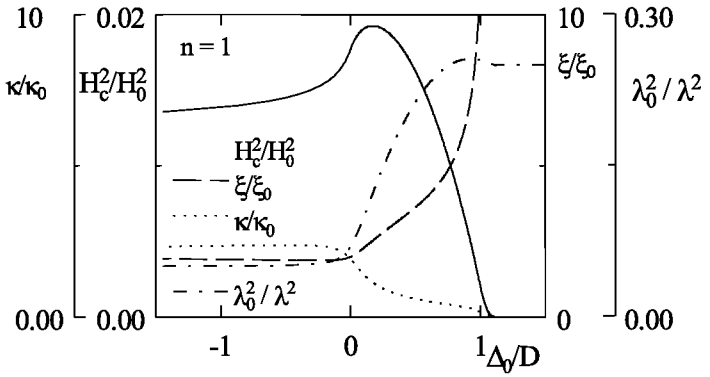

Fig. 4. The plots of H_c^2, ξ, $1/\lambda^2$ and κ as a function of Δ_0/D at $T = 0$ for $n = 1$, $I_0/2D = 0.1$, $J_0/2D = 0.05$, $-\infty \leq U_d \leq 0$, $U_c = U_{cd} = 0$. $H_0^2 = 16\pi D/a^3$, $\xi_0 = a/4\sqrt{2}$, $\lambda_0^2 = \hbar^2 c^2 az/16\pi e^2 D$, $\kappa_0 = \left(\sqrt{2}\hbar c/\sqrt{\pi}e\right)(1/\sqrt{aD})$, $D = zt$.

the factor 40) for $n < 2$. Also their concentration dependences are very different (comp. Fig. 3b with Fig. 3a).

The crossover between the local-pair-like and BCS-like behavior is clearly seen in the variation of ξ, κ, and $1/\lambda^2$ with increasing Δ_0 (cf. Fig. 4). For $\Delta_0 \leq 0$, $\xi(\kappa)$ is very small (large), indicating extreme type II superconductivity, and $\xi(\kappa)$ rapidly increases (decreases) as one approaches the c-regime at $\Delta_0/D \approx n$. The London penetration depth $\lambda(0)$ being very large in the local pair limit ($\Delta_0 < 0$) decreases with increasing Δ_0 in $d+c$ regime, whereas in c-regime it remains almost constant.

Figure 5 shows the variation of the ratio $2k_B T_c/E_g^{\min}(0)$ as a function of Δ_0/D for $n = 1$, $J_0 = 0$ and a fixed value of $I_0/2D$ in the cases of $U_d \to -\infty$ and $U_d = 0$. As we see the ratio approaches the BCS value in c-regime and it strongly

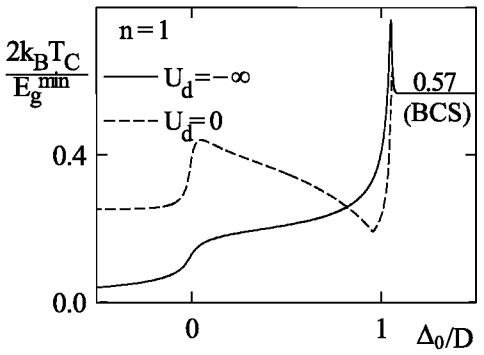

Fig. 5. The variation of the ratio $2k_B T_c/E_g^{\min}(0)$ as a function of Δ_0/D for $U_d = -\infty$ and $U_d = 0$ at $n = 1$, where $E_g^{\min}(0) = \min\{E_g^c(0), E_g^d(0)\}$, plotted for $I_0/2D = 0.1$, $J_0 = U_c = U_{cd} = 0$.

decreases as the concentration of d-electrons increases above that of wide band electrons with decreasing Δ_0.

The Coulomb interactions U_{cd}, U_c can strongly influence the concentration dependences of superconducting characteristics both in the local pair (d) regime as well as in the mixed ($d+c$) regime.

In Fig. 6 we show the evolution of the London penetration depth ($1/\lambda^2$) at $T = 0$ as a function of total electron concentration n for various values of intersubsystem Coulomb repulsion U_{cd} and two fixed values of Δ_0/D, whereas Fig. 7 shows examples of the plots of $1/\lambda^2$ as a function of Δ_0 for the fixed values of n and U_{cd}. Both these figures are calculated for $I_0/2D = 0.1$, $J_0 = 0$,

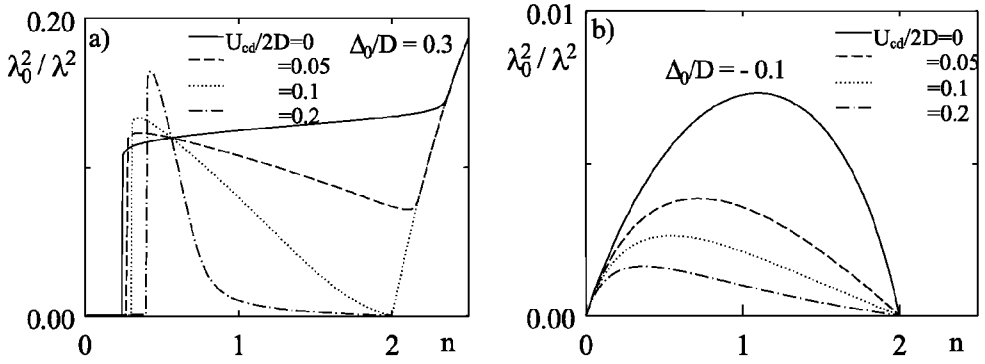

Fig. 6. The inverse square of penetration depth λ^{-2} at $T = 0$ as a function of total concentration of carriers n for different values of Δ_0/D and interaction $U_{cd}/2D$. $I_0/2D = 0.1$, $J_0 = U_c = 0$, $-\infty \leq U_d \leq 0$, $U_{cd}/2D = 0$, 0.05, 0.1, 0.2. $\lambda_0^2 = \hbar^2 c^2 az/16\pi e^2 D$; (a) $\Delta_0/D = 0.3$, (b) $\Delta_0/D = -0.1$.

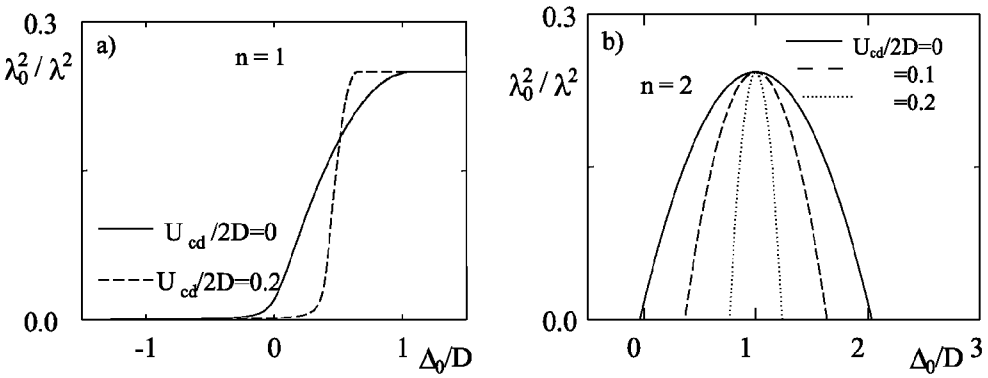

Fig. 7. The inverse square of penetration depth λ^{-2} at $T = 0$ as a function of Δ_0/D for different values of n and interaction $U_{cd}/2D$. $I_0/2D = 0.1$, $J_0 = U_c = 0, -\infty \leq U_d \leq 0$; $\lambda_0^2 = \hbar^2 c^2 az/16\pi e^2 D$; (a) $n = 1$, $U_{cd}/2D = 0$, 0.2, (b) $n = 2$, $U_{cd}/2D = 0$, 0.1, 0.2.

$-\infty \leq U_d \leq 0$, as the ground state diagrams given in Fig. 2a. Figure 6a is plotted for $\Delta_0/D = 0.3$. In this case upon increasing n one observes two change-overs: BCS→MIXED→BCS (comp. the diagrams 2a and Fig. 3a). On the contrary, for $\Delta_0/D = -0.1$ (Fig. 6b) the superfluid characteristics for any $n < 2$ are dominated by the d-subsystem ($n_d \gg n_c$), comp. Figs. 2a and 3b. In comparison to the former case $1/\lambda^2$ is strongly reduced (up to the factor 20) and shows a quite different concentration dependence. Also the effects of U_{cd} on $\lambda(n)$ are different in both cases.

The superconducting critical temperature T_c as a function of Δ_0 is influenced by U_c and U_{cd} in the following way. The repulsive U_c shifts the maximum of T_c towards higher values of Δ_0. This is simply a consequence of extending the coexistence region of d and c electrons by U_c (cf. Figs. 1c, 2b). The effect of U_{cd} is different: there is no essential shift of the maximum T_c versus Δ_0, and the coexistence region is reduced. Examples of the plots of T_c vs. Δ_0/D are shown in Fig. 8 for $n = 2$ and a few fixed values of U_c and U_{cd}.

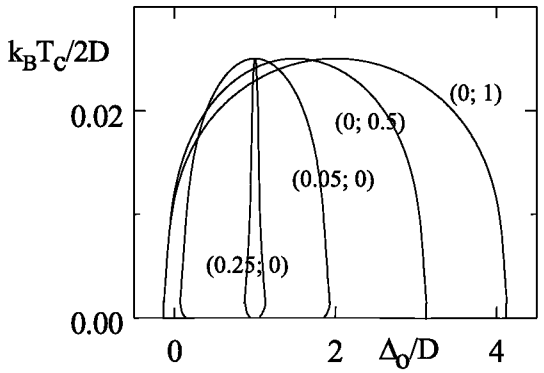

Fig. 8. The superconducting critical temperature as a function of Δ_0/D for $J_0/2D = 0.05$, $I_0 = 0$, $n = 2$, $U_d/D = -\infty$. The values of U_c and U_{cd} are given in the brackets $(U_{cd}/2D;\ U_c/2D)$ next to the curves.

Closing this section let us shortly conclude the effects of on-site density interaction U_d, being the main factor determining the d-pair binding energy E_b^d (for a more detailed discussion see Refs. [1, 2, 11]).

For $U_d \leq 0$, decreasing $|U_d|$ yields a moderate reduction of T_c in comparison to the $U_d = -\infty$ case (up to a factor 2 for $U_d \to 0$). As we see from Fig. 5 the ratio $k_B T_c/E_g^{\min}(0)$ is substantially enhanced by a decrease in $|U_d|$ in the d (LP) regime and it can be either enhanced or reduced in the $c + d$ (MIXED) regime. In the c regime $k_B T_c/E_g^{\min}(0)$ remains almost unaffected by U_d and it approaches the BCS value (0.57) for any $U_d \leq 0$.

The *repulsive* U_d competes both with I_0 and J_{ij} and its effects on the properties of the system can be much more spectacular than those of $U_d < 0$. In general, for a weak repulsion the superconducting transition remains continuous, as for

$U_d < 0$, however the d-pair density exhibits a sharp break at T_c. The T_c, $H_c^2(0)$, κ, and (for $I_0 \neq 0$) the ratio $k_B T_c / E_g^c(0)$ is strongly reduced, whereas the G–L coherence length is enhanced. The increasing U_d changes the nature of the phase transition from a continuous to a discontinuous type, resulting in the tricritical point (TCP), then it suppresses superconductivity for high n_d ($|n_d - 1| \approx 1$). Finally, for a large U_d the system remains in the normal state at any temperature and any n_d [2, 11].

4. Final remarks

We have studied the thermodynamic and electromagnetic properties and phase diagrams of an induced pairing model. The model considered assumes arbitrary value of the on-site density interaction between localized d-electrons U_d, which allows investigation of the effects of reduced d-pair binding energy. Moreover, it takes into account the Coulomb interactions between itinerant electrons U_c and those between c and d electrons U_{cd} as well as the direct pair hopping interaction J_{ij}.

Depending on parameters the model is found to exhibit several kinds of superconducting behavior ranging from the BCS-like to the local-pair-like. In particular, for $I_0 \neq 0$, $U_d \leq 0$ and fixed n the electromagnetic properties like ξ, H_c, λ, κ as well as the ratio $k_B T_c / E_g^{\min}(0)$ can evolve with the position of LP level (Δ_0) from LP to "Crossover" (MIXED) and finally to BCS-like regime. There are also three possible types of change-overs with an increasing total number of carriers: BCS$\longrightarrow$MIXED$\longrightarrow$BCS, BCS$\longrightarrow$LP and LP$\longrightarrow$BCS.

As we found, the Coulomb interactions U_c and U_{cd} can substantially change the ground state diagrams of the model and strongly modify the evolution of basic superconducting characteristics with particle concentration and Δ_0. The intrasubsystem Coulomb interaction U_c enlarges the coexistence region of c and d particles (MIXED regime). On the contrary, the intersubsystem Coulomb repulsion U_{cd} tends to reduce the MIXED region and the range of n in which both types of particles coexist.

There are various groups of materials for which the coexistence of local pair states with itinerant electron states have been either established or suggested and which can be suitable candidates for the present model [3–9, 12]. Among these materials there are also several nonstandard ("exotic") superconductors, including the high-T_c cuprates, the tungsten bronzes and the doped bismuthates ($Ba_{1-x}K_xBiO_3$ and $BaPb_{1-x}Bi_xO_3$).

For the bismuthates the experimental results show the existence of p-holes together with disproportionated (at least locally) $Bi^{3+}-Bi^{5+}$ background [13, 14], and the coexistence of itinerant carriers with small bipolarons has been indicated by the Raman spectroscopy data [15]. The existence of local electron pairing is also supported by several photoemission studies, which provide the evidences of a pseudogap behavior in the normal state of these materials [16].

Recently Puchkov et al. [17] have analyzed the doping dependence of the optical properties of $Ba_{1-x}K_xBiO_3$ in the full doping range ($0 < x \leq 0.46$). In contrast to the cuprates the London penetration depth has been found to be almost doping independent in an extended range of x, i.e. it exhibits the behavior analogous to that corresponding to $\Delta_0/D = 0.3$ in Figs. 3a and 6a. This suggests that the system considered is in the $c + d$ (MIXED) regime for a wide range of doping. Support for such a conclusion is provided by the experimental finding that in doped $BaBiO_3$ the density of the itinerant (Drude) charge carriers does not significantly change with doping [17]. Within our theory such a result is easy to explain by a strong pinning of chemical potential μ around the d-level (Δ_0) in the MIXED regime, which yields the itinerant carriers concentration n_c to be almost n-independent.

A more detailed discussion on the relevance of the induced pairing model to the interpretation of experimental data for the cuprates will be given elsewhere [11].

Acknowledgments

We would like to thank R. Micnas, J. Ranninger, M.C. Ren and P. van Dongen for valuable discussions and comments. This work was supported in part by the State Committee for Scientific Research with the project 2 P03 B037 17.

References

[1] W. Czart, M. Szkudlarek, S. Robaszkiewicz, *Acta Phys. Pol. A* **91,** 415 (1997).

[2] G. Pawłowski, S. Robaszkiewicz, *Mol. Phys. Rep.* **12,** 191 (1995); *idem*, *Acta Phys. Pol. A* **94,** 683 (1998).

[3] J. Ranninger, S. Robaszkiewicz, *Physica B* **135,** 468 (1985).

[4] S. Robaszkiewicz, R. Micnas, J. Ranninger, *Phys. Rev. B* **46,** 180 (1987).

[5] R. Micnas, J. Ranninger, S. Robaszkiewicz, *Rev. Mod. Phys* **62,** 113 (1990).

[6] J. Ranninger, J.M. Robin, *Physica C* **253,** 279 (1995); J. Ranninger, J.M. Robin, M. Eschrig, *Phys. Rev. Lett.* **74,** 4027 (1995); P. Devilard, J. Ranninger, *Phys. Rev. Lett.* **84,** 5200 (2000); H.C. Ren, *Physica C* **303,** 115 (1998).

[7] R. Friedberg, T.D. Lee, M.C. Ren, *Phys. Rev. B* **42,** 4122 (1990); *ibid. B* **45,** 10732 (1992); E. Piegari, V. Cataudella, G. Iadonisi, *Physica C* **303,** 273 (1998).

[8] V.B. Geshkenbein, L.B. Ioffe, A.I. Larkin, *Phys. Rev. B* **55,** 3173 (1997); C.P. Enz, *Phys. Rev. B* **54,** 3589 (1996).

[9] R. Micnas, S. Robaszkiewicz, in: *High-T_c Superconductivity 1996; Ten Years after the Discovery*, Eds. E. Kaldis, E. Liarokapis, K.A. Müller, *NATO ASI Series E*, Vol. 342, Kluwer Academic Publ., Dordrecht 1997, p. 31 and references therein; R. Micnas, S. Robaszkiewicz, B. Tobijaszewska, *J. Supercond.* **12,** 79 (1999).

[10] S. Robaszkiewicz, G. Pawłowski *Physica C* **210,** 61 (1993); S. Robaszkiewicz, *Acta Phys. Pol. A* **85,** 117 (1994).

[11] W.R. Czart, S. Robaszkiewicz, unpublished.

[12] J.A. Wilson, *Physica C* **233,** 332 (1994); J.A. Wilson, A. Zahir, *Rep. Prog. Phys.* **60,** 941 (1998).

[13] C.L. Lin, S.L. Qiu, Jie Chen, Myron Strongin, Gang Cao, ChanSoo Jee, J.E. Crow, *Phys. Rev. B* **39,** 9607 (1989).

[14] C.H. Rüscher, H. Heinrich, W. Urland, *Physica C* **219,** 471 (1994); E.S. Hellman, E.H. Hartford Jr., *Phys. Rev. B* **52,** 6822 (1995).

[15] S. Sugai, *Solid State Commun.* **72,** 1187 (1990).

[16] S. Tajima, S. Uchida, A. Masaki, H. Takagi, K. Kitazawa, S. Tanaka, S. Sugai, *Phys. Rev. B* **35,** 696 (1987); J.B. Boyce, F.G. Bridges, T. Claeson, T.H. Geballe, G.G. Li, A.W. Sleight, *Phys. Rev. B* **44,** 6961 (1991); M.A. Karlow, S.L. Cooper, A.L. Kotz, M.V. Klein, P.D. Han, D.A. Payne, *Phys. Rev. B* **48,** 6499 (1993); H. Namatame, A. Fujimori, H. Torii, T. Uchida, Y. Nagata, J. Akimitsu, *Phys. Rev. B* **50,** 13674 (1994).

[17] A. Puchkov, T. Timusk, M.A. Karlow, S.L. Cooper, P.D. Han, D.A. Payne, *Phys. Rev. B* **54,** 6686 (1996).